Astron. Astrophys. 288, 457–465 (1994)

ASTRONOMY AND ASTROPHYSICS

Size and physical conditions of the coronal line region in a nearby Seyfert 2: the Circinus galaxy*

E. Oliva[1], M. Salvati[1], A.F.M. Moorwood[2], and A. Marconi[3]

[1] Osservatorio Astrofisico di Arcetri, Largo E.Fermi 5, I-50125 Firenze, Italy
[2] European Southern Observatory, Karl Schwarzschild str. 2, D-85748 Garching bei München, Germany
[3] Università degli Studi di Firenze, Dip. di Astronomia e Scienza dello Spazio, Largo E.Fermi 5, I-50125 Firenze, Italy

Received 17 November 1993 / Accepted 11 February 1994

Abstract. We present observations of visible ([Fe VII], [Fe X], [Fe XI], [S VIII]) and near infrared ([S IX], [Si VI], [Ca VIII], [Si VII], [Si IX]) coronal lines in the Circinus galaxy. The number of detected lines, their velocity profiles, and their spatial distribution pose tight constraints on models of the coronal line region (CLR), and lead to several important conclusions. We can exclude fast shocks and hot stars (warmers) as the origin of the coronal line emission, and find convincing (although not conclusive) evidence against a hot, collisionally ionized plasma. The CLR appears to be a dense ($N_e \simeq 250$ cm^{-3}), compact (diameter $\simeq$10 pc), dustless region photoionized by the nuclear continuum which must be remarkably flat ($L_\nu \approx \nu^{-0.5}$) around 300 eV.

Key words: line: formation – line: identification – galaxies: active – galaxies: individual: Circinus – galaxies: nuclei – infrared: galaxies

1. Introduction

Coronal lines are forbidden transitions within the ground terms of highly ionized species ($h\nu_{ion} \geq 100$ eV) which can be formed either in gas photoionized by a hard UV continuum or in a very hot, collisionally ionized plasma. Although lines of [Fe VII] and [Fe X] have been long known to be common features in the visible spectra of AGN, the physical conditions of the emitting region are still poorly known and much debated.

Photoionization seems an obvious mechanism in AGNs as the ionizing continuum is very hard and extends well beyond 100–300 eV, the ionization thresholds of the observed species. Very high values of the ionization parameter $U = Q(\mathrm{H})/(4\pi R^2 N_e c) \sim 1$ (e.g. Davidson & Netzer 1979) are required, however, to keep most of iron in the form of Fe VII–Fe XI. The key quantity is the gas density which sets the maximum distance beyond which the geometric dilution of the ionizing field prevents the formation of coronal species. If the CLR is dense it must be located very close to the nucleus. If on the contrary it is more diffuse ($N_e \approx 1$ cm^{-3}, as suggested by Korista & Ferland 1989, hereafter KF89) it may extend over a distance comparable to the size of the extended narrow line regions.

Alternatively, in the case of collisional ionization, the gas must have $T \sim 10^6$ K and such a hot plasma could be the confining medium for the clumps forming the NLR (Oke & Sargent 1969). The best method to verify this hypothesis would be to measure the electron temperature which is expected to be much lower, $T_e \simeq 3 \cdot 10^4$ K, if the gas is photoionized (e.g. Grandi 1978). Ratios between UV lines from high lying ($E_u > 9 \cdot 10^4$ cm^{-1}) levels and visible/infrared transitions from the same coronal ion could, in principle, be used for this purpose. Unfortunately, the well known Fe VII, Fe X, Fe XI ions have no suitable pair of lines (Penston et al. 1984) and it is therefore of interest to search for other ions which could provide convenient thermometers. Less direct evidence for/against collisional ionization is provided by theoretical computations of line ratios in a hot plasma. From the visible Fe lines alone it is known that the coronal gas cannot be at a single temperature but must consist of several components at different T with no gas hotter than $\approx 5 \cdot 10^6$ K (Nussbaumer & Osterbrock 1970, hereafter NO70). Using lines from many ions one can tighten the constraints on the temperature distribution and, most important, verify if a solution exists at all.

Coronal ions can also be formed inside a 'normal' NLR when bulk motions (infall or outfall) induce strong shocks in the NLR clouds. If the shocks are faster than $\simeq$ 300 km/s they can produce a column density of coronal ions compatible with the observed luminosities of [Fe X] (Viegas-Aldrovandi & Contini 1989). The excitation mechanism is a mixture of collisional ionization at the shock front and photoionization in the pre/postshock regions (Contini & Viegas 1992 and references therein) and there is no simple way of verifying if shock ex-

Send offprint requests to: E. Oliva

* Based on observations collected at the European Southern Observatory, La Silla, Chile

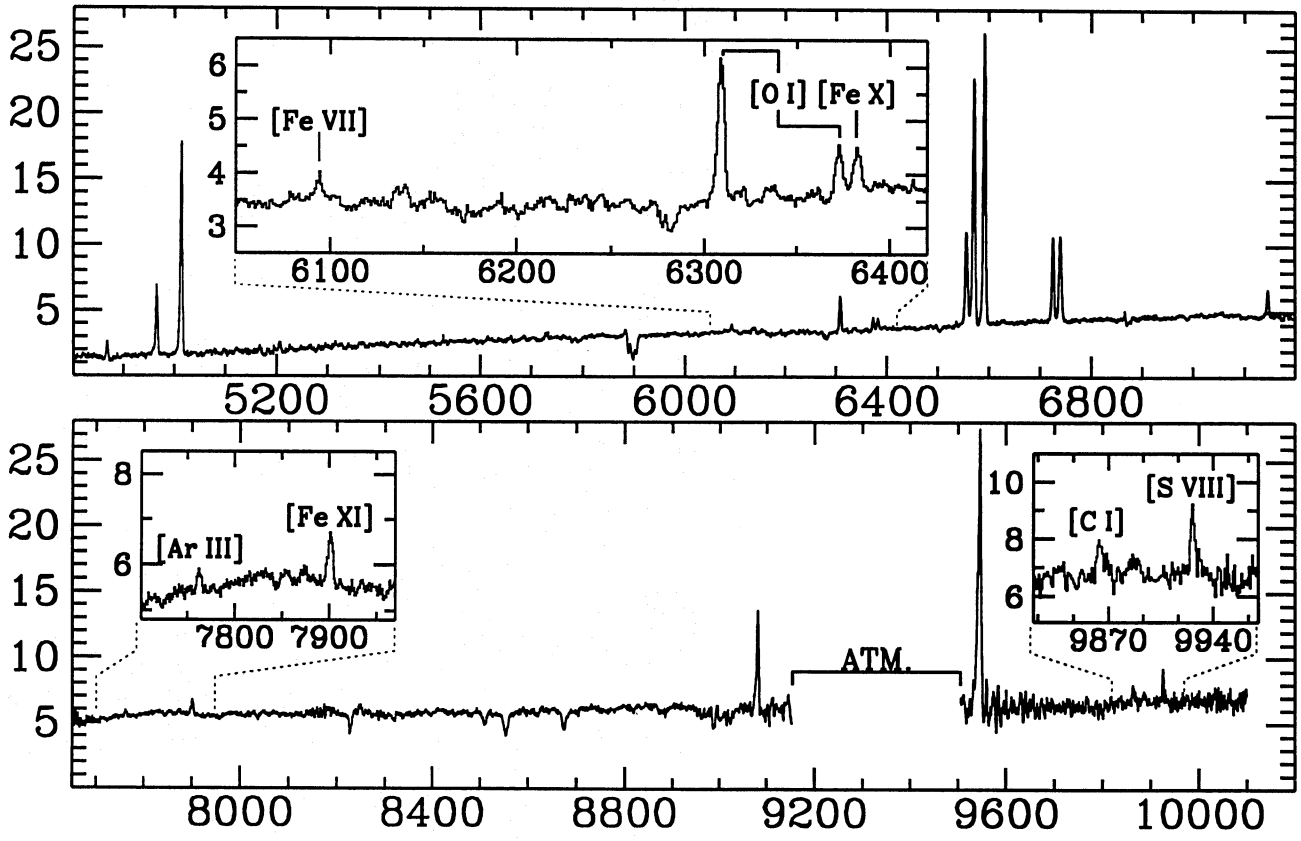

Fig. 1. EMMI spectrum of the central 1.5"x4.5" of the Circinus galaxy. Wavelengths are in Å and fluxes in units of 10^{-15} erg cm^{-2} s^{-1} Å^{-1}. 'ATM' is a region of bad atmospheric transmission

citation is important unless one finds objects with lines much narrower than 300 km/s.

The Circinus galaxy (A1409-65) is a nearby ($\simeq$ 4Mpc) isolated spiral of type Sb-Sd which lies close to the galactic plane but in a region of relatively low ($A_V \simeq 1.5$ mag.) interstellar extinction (Freeman et al. 1977). Evidence of unusual nuclear activity was first provided by its discovery as an H_2O megamaser (Gardner & Whiteoak 1982). Subsequent studies revealed an infrared luminosity of $\simeq 10^{10}$ $L_\odot$ and overall infrared energy distribution, including 3.28μm emission and 9.7μm absorption features, characteristic of starburst activity but a large [N II]/H_α ratio and compact infrared nucleus indicative of a Seyfert nucleus (Moorwood & Glass 1984; Moorwood & Origlia 1990). Infrared spectroscopy has revealed a strong stellar continuum with deep CO absorption bands, H, H_2 and [FeII] emission lines characteristic of both starburst and Seyfert galaxies (Moorwood & Oliva 1988), and prominent [Si VI] which confirms the presence of a Seyfert nucleus (Moorwood & Oliva 1990, 1993a).

In this paper we present visible and infrared spectral observations aimed at clarifying the origin of the coronal lines and the physical conditions of the CLR.

2. Observations

The infrared data were collected in September 1992 and April 1993 using the ESO long slit spectrometer IRSPEC (Moorwood et al. 1991) mounted on the ESO-NTT telescope. The detector was a SBRC 62x58 InSb array whose pixels subtend 2.2" along the slit and correspond to $\simeq$ 2 Å at 1.25 μm, $\simeq$ 5 Å at 2 μm, $\simeq$ 10 Å at 4 μm along the dispersion. The slit width was 4.4" (2 pixels) yielding a resolving power of $R = 2000 - 3000$ depending on wavelength. The observations consisted of several pairs of object and sky frames spaced by 2 minutes. On-chip integration time was 60 sec at $\lambda < 2.5$ μm and 0.6 sec at 4 μm. The data were reduced using the IRSPEC context in MIDAS, the ESO reduction package. The spectra were wavelength calibrated to better than 20 km/s using OH sky lines (Oliva & Origlia 1992) or a Neon lamp, and corrected for atmospheric and instrumental transmission using measurements of featureless, early O stars. Absolute flux calibration was derived from observations of photometric standard stars.

The optical spectra were collected in April 1991 using the 600 grooves/mm grating of EMMI mounted on the ESO-NTT. The projected pixel size of the Ford 2024^2 CCD was 0.35" along the slit and $\simeq$ 0.8 Å along the dispersion. The slit width was 1.5", yielding $R \simeq 2000$ at 7000 Å. A 4500–10000 Å spectrum was obtained by merging 5 exposures of 1000 sec. at different grating positions. Data reduction was performed using standard procedures for long-slit CCD spectra and the wavelength calibration was optimized using sky lines (Osterbrock & Martel 1992). For both the optical and IR measurements the slit was

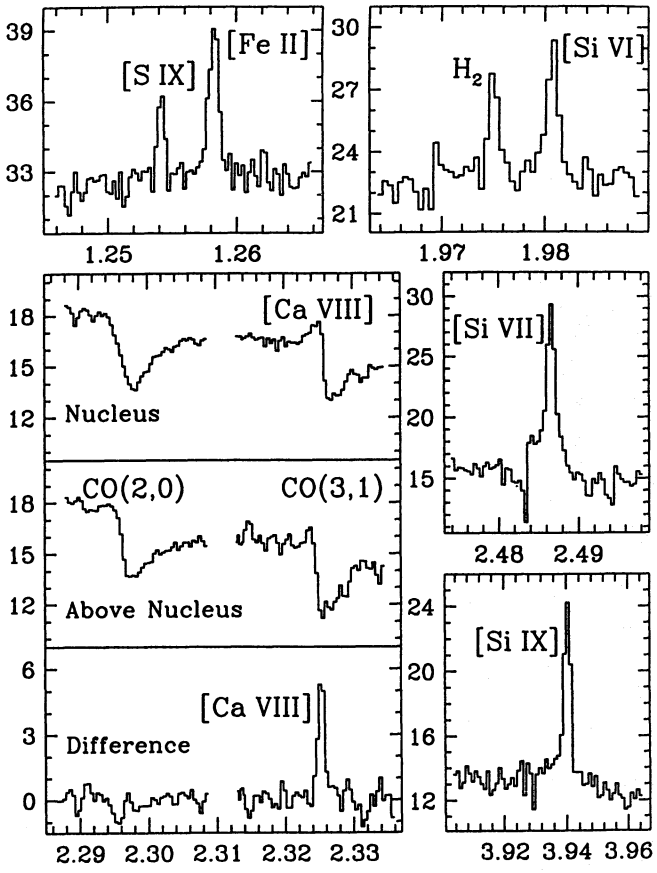

Fig. 2. IRSPEC spectra at selected grating positions around coronal lines. Wavelengths are in μm and fluxes, in a 4.4"x6.6" beam, are in units of 10^{-11} erg cm^{-2} s^{-1} μm^{-1}. Nuclear and extra–nuclear spectra around [Ca VIII] are also displayed to show how the stellar continuum was subtracted (Sect. 3)

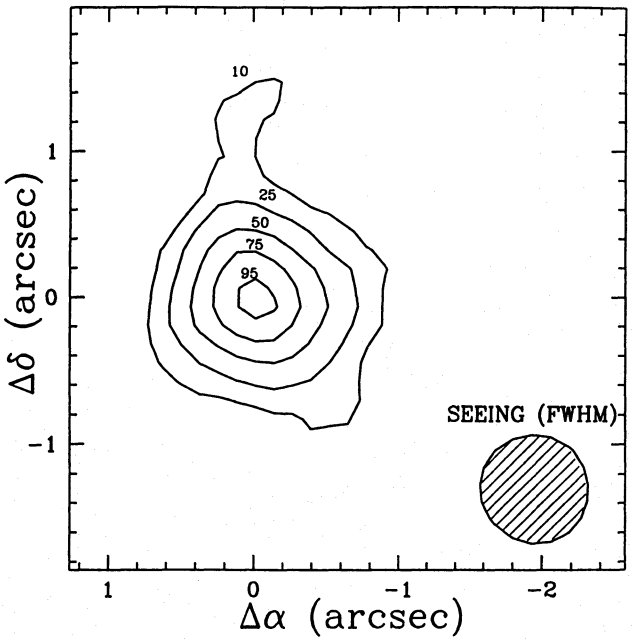

Fig. 3. Continuum subtracted image in [Fe XI], north is top and east is left. Contour levels are in percent of the peak intensity

set at P.A. 160^o. More details of the data reduction can be found in Marconi (1993).

An image in [Fe XI] λ7892 was taken in April 1993 using SUSI (ESO-NTT) with narrow band (FWHM$\simeq$ 70 Å) filters centered at 7880 Å (ESO #415) and 7027 Å (ESO #443). The seeing was 0.75" and several 15 min frames were co-added for each filter. Data reduction was standard, i.e. bias and sky subtraction, flat–fielding and relative flux calibration. The correct subtraction of the very red galactic continuum was verified on an annular region 5–10" from the nucleus where, on the basis of our long-slit spectra, there is no line emission and the continuum spectral shape is the same as on the nucleus.

3. Results

The optical spectrum is displayed in Fig. 1 and a mosaic of the infrared spectra is shown in Fig. 2. To our knowledge this is the first extragalactic measurement of [Si IX] (3.935μm) and the first astronomical detection of [S IX] (1.252μm). Although this line is blended with He I λ1.2527 ($3\,^3S$-$4\,^3P^o$) and [Fe II] λ1.2521 ($a\,^6D_{3/2}$-$a\,^4D_{1/2}$) their contributions are negligible because He I λ1.2527/λ1.083<0.005 (Smits 1991) and [Fe II] λ1.2521/λ1.2567<0.02 (from our upper limit on [Fe II] λ1.5995). The lines of [Si VI], [Si VII] and marginal [Ca VIII] were previously detected in NGC1068 (Oliva & Moorwood 1990; Moorwood & Oliva 1991; Moorwood & Oliva 1993a), while [S VIII] was tentatively identified in NGC4151 by Osterbrock et al. (1990) and later confirmed by Reconditi & Oliva (1993, hereafter RO93).

Measurement of the [Ca VIII] line is complicated by the deep CO Δv = 2 bands produced in the atmospheres of red (super)giant stars which dominate the emission around 2.3μm. As shown in Fig. 2, however, this continuum could be adequately removed by subtracting the spectrum obtained 5" above the nucleus (after shifting it in wavelength to compensate for the galaxy rotation and scaling it to the nuclear continuum level).

The observed line parameters are summarized in Table 1. Although the atmospheric transmission at the rest wavelengths of [Si VI] and [Si VII] is quite low, the redshifted positions of these lines fall in the middle of narrow and relatively clean windows. We also took advantage of the different heliocentric corrections at the two epochs of observation (+6 and -18 km/s) to make sure that part of the lines were not hidden in atmospheric absorption features much narrower than our resolution (see also RO93). The intensities were corrected for extinction using the observed ratios of [FeII] (Oliva et al. 1989) and hydrogen recombination lines. These ratios are all consistent with $A_V = 5.2 \pm 0.4$ and do not show any significant deviation from the standard reddening curve.

Fluxes of the visible and infrared coronal lines are directly comparable as the CLR is smaller than the slit used in the spectrographs (1.5" optical and 4.4" infrared). For the lower excitations lines the difference in beam sizes has been corrected for

Table 1. Observed line parameters

Line[1]	$F^{(2)}_{-15}$	$I^{(3)}_{-15}$	$I^{(4)}_{REL}$	$\Delta v^{(5)}$
HeII λ4687	1.3	490	33.	–3
Hβ	5.7	1650	110.	+1
[O III] λ4959	26	6600	440.	+3
[O III] λ5007	83	19500	1300.	+6
[N I] λλ5198,5200	3.2	580	39.	–
*[Fe XIV] λ5303	<1	<160	<11	–
*[Fe VII] λ6087	1.4	90	6.0	–10
[O I] λ6300	11.5	600	40.	+2
[O I] λ6364	3.6	180	12.	0
*[Fe X] λ6374	3.5	170	11.	–29
[N II] λ6548	44	1840	123.	+1
Hα	109	4490	300.	–9
[N II] λ6583	130	5260	351.	0
[S II] λ6716	38	1370	92.	+5
[S II] λ6731	37	1320	88.	+4
[Ar III] λ7136	10	265	18.	–1
[O II] λλ7320,7330	5.3	120	8.0	–
[Ar III] λ7751	3.5	60	4.0	–3
*[Fe XI] λ7892	6.9	110	7.3	–49
[S III] λ9069	43	380	25.	–2
[S III] λ9531	156	1160	78.	–4
[C I] λ9850	5.3	35	2.3	+8
*[S VIII] λ9913	11	72	4.8	–31
He I λ1.0830	160	800	40.	–6
*[S IX] λ1.25235[a]	20	69	4.6	–35[a]
[Fe II] λ1.2567	59	205	10.	–9
Paβ	104	340	17.	-12
[Fe II] λ1.5995	<20	<50	<2.5	–
[Fe II] λ1.6435	70	150	7.5	+7
H_2 λ1.9570	59	105	5.3	–3
*[Si VI] λ1.963	82	145	9.7	–43
H_2 λ2.1213	79	130	6.5	+9
Brγ	38	61	3.0	–10
*[Ca VIII] λ2.321	70	107	7.1	–35
*[Si VII] λ2.483	160	233	16.	–28
*[Si IX] λ3.9346[a]	260	308	21.	–35[a]
Brα	150	180	8.7	–

Notes to Table 1

(1) Rest wavelengths are in Å for $\lambda < 1\ \mu m$ and in μm beyond. Positions of coronal lines (marked with *) are from Fuhr et al. (1988) and RO93. The wavelengths of S IX and Si IX are determined here (note *a*).

(2) Observed line flux, units of 10^{-15} erg cm^{-2} s^{-1}.

(3) Extinction corrected flux, same units.

(4) Relative intensities scaled to Hα=300. Low excitation IR lines were beam corrected adopting case B hydrogen line ratios, this correction was not applied to coronal lines as the CLR is smaller than the optical aperture.

(5) Line center position (km/s) relative to +465 km/s.

[a] Newly determined line positions (Δv=-35 assumed). The accuracy is ±4 Å (Si IX) and ±1.4 Å (S IX).

by imposing case B ratios for the hydrogen lines (column 4 of Table 1).

Figure 4 shows intensity contour plots in the position–velocity plane for selected optical lines. Note the different kinematic behaviour of [N II] and [O I], which display a typical rotation pattern, and [Fe X] and [Fe XI] which do not show any sign of rotation and are spatially unresolved. All the visible and IR coronal lines are quite narrow and only barely resolved at the instrumental limit of 150 km/s implying intrinsic widths of $\leq$ 100 km/s.

The size of the region emitting the highest excitation lines can be estimated from the [Fe XI] image (Fig. 3) which yields a deconvolved FWHM of about 0.6" or 10 pc at a distance of 4 Mpc. The other coronal lines are also strongly concentrated towards the nucleus and are spatially unresolved in the long slit spectra at a limit slightly lower than 2".

The visible coronal lines are blue-shifted (by about 35 km/s) with respect to other lines (Fig. 4 and Table 1, a similar effect was found by Penston et al. 1984 in their observations of [Fe X] in several AGNs). Those infrared coronal lines whose wavelengths are already accurately known also exhibit the same blueshift. An explanation of this in terms of dust extinction is thus difficult, particularly given the additional argument against the presence of significant amounts of dust in the CLR based on abundances discussed below. All lines from lower excitation species seen with sufficient s/n ratio (i.e. Hα, Hβ, [O III], [S III], [Ar III], [S II], [O I]) also exhibit the asymmetrical profiles with blue wings often seen in Seyfert 2 galaxies (Fig. 4 and Marconi 1993).

4. Discussion

4.1. Physical conditions in the CLR

4.1.1. Gas density

The density can be related to the observed flux and spatial extent of the coronal lines by

$$\sigma = N_e\, N(\mathrm{Fe}^{+10})\, f\, \theta\, D\, \epsilon(\mathrm{Fe}^{+10}) \quad \mathrm{erg\ cm^{-2}\ s^{-1}\ arsec^{-2}} \qquad (1)$$

where σ is the surface brightness of [Fe XI], N_e, $N(\mathrm{Fe}^{+10})$ are the number densities of electrons and Fe^{+10} ions, f is the filling factor, θ is the angular diameter of the CLR, D is the distance to the object and $\epsilon(\mathrm{Fe}^{+10})$ is the line emission coefficient. This latter is a function of temperature alone as long as $N_e \ll 5 \cdot 10^9$ cm^{-3} (the critical density of the upper level), which is always the case for the conditions of interest here. Using the collision strengths of Mason (1975) and $T_e = 3 \cdot 10^4$ K, typical of a photoionized CLR, one finds $\epsilon(\mathrm{Fe}^{+10}) = 5.0 \cdot 10^{-21}$ erg cm^3 s^{-1} which yields

$$\sigma = 4.7 \cdot 10^{-18} N_e^2\, f \left[\frac{\theta}{0.6"}\right]\left[\frac{D}{4\mathrm{Mpc}}\right]\left[\frac{x(\mathrm{Fe}^{+10})}{0.3}\right]\left[\frac{A(\mathrm{Fe})}{4.7\ 10^{-5}}\right] \qquad (2)$$

where $x(\mathrm{Fe}^{+10}) = N(\mathrm{Fe}^{+10})/N(\mathrm{Fe})$ is the average fraction of iron in the form of Fe XI and A(Fe) is the iron abundance normalized to its cosmic value and without dust depletion. The dereddened flux and spatial extension of [Fe XI] give $\sigma \simeq 3.1 \cdot 10^{-13}$ erg cm^{-2} s^{-1} arcsec^{-2} which, inserted in Eq. 2, yields $N_e^2\, f \simeq 6.5 \cdot 10^4$ cm^{-6} with the normalized abundances of Eq. 2 set to

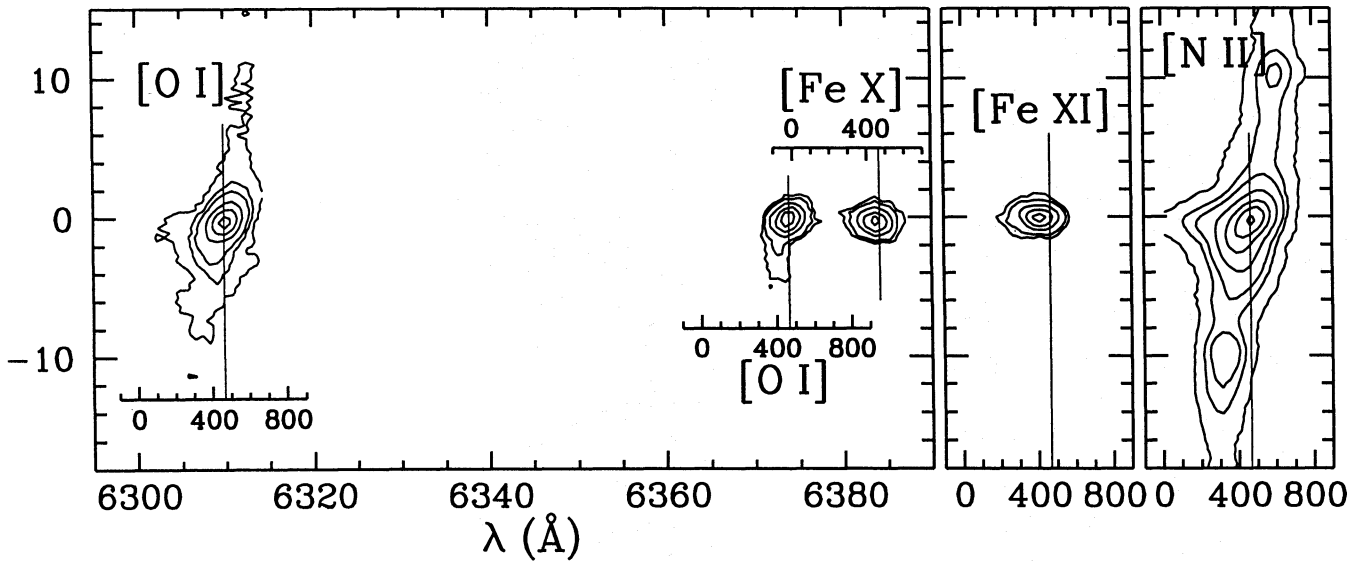

Fig. 4. Intensity contour plots in the position–velocity plane for selected optical lines. The ordinate gives the relative position (in arc–sec) along the slit which is at P.A.=160°, i.e. N is down. The velocity scales are in km/s and the vertical bars are at +465 km/s. Levels are normalized to 100, 75, 50, 25, 15, 5, and 1 percent of the highest contour, lowest levels are shown only when above the noise. Note that [O I] λ6364 and [Fe X] λ6374 have the same peak intensity and their different shapes cannot be attributed to s/n effects

unity. It is therefore clear that the CLR is quite dense: $N_e \sim 250$ cm^{-3} $f^{-1/2}$.

The above reasoning can easily be extended to a CLR formed by a collisionally ionized gas with $T_e \approx 10^6$ K. At these temperatures the line is mostly produced by electron collisions to high lying levels and subsequent cascade to the ground state and one finds $\epsilon(Fe^{+10}) \simeq 1.1 \cdot 10^{-20}$ erg cm^3 s^{-1} (Mason 1975, see also Sect. 4.3), a factor 2.2 larger than at $3 \cdot 10^4$ K. The resulting density is therefore a factor 1.5 lower, i.e. $N_e \sim 170$ cm^{-3} $f^{-1/2}$, but still quite large.

It is worth noting that the contribution of electric dipole continuum pumping of [Fe XI] (cf. Fig. 1 of KF89) is negligible due to the narrow width of the lines. Even assuming that all the continuum photons within 100 km/s (the observed line width) of the UV pumping lines are absorbed by Fe XI one finds that only a fraction $< 10^{-4}$ of the ionizing photons can be converted into [Fe XI], which corresponds to less than 4% of the observed line flux. This conclusion is also confirmed by photoionization models computed with CLOUDY (Ferland 1993).

4.1.2. Gas temperature

Based on a detailed analysis of the UV transitions from the observed ions it appears that the most promising thermometers are [Si VII] λ1049/λ2.483 and [Si IX] λ950/λ3.935 which vary respectively from 0.04 to 0.89 and from 0.02 to 0.55 between $T = 3 \cdot 10^4$ and $T = 10^6$ K. Measurements of these relatively faint UV lines could give a definite answer on the role of collisional ionization but are probably unfeasible in Circinus because of its relatively high extinction.

4.1.3. Pressure in the coronal and narrow line regions.

From the [S II] line ratio and Hα surface brightness it can be deduced that the NLR clumps have $f \sim 0.1$ and $N_e = 450^{+250}_{-150}$ which, for a typical temperature of 8000 K, yields a pressure $N_e T \simeq 4 \cdot 10^6$. In the CLR $N_e T \approx 7 \cdot 10^6 f^{-1/2}$ if the gas is photoionized and 20 times larger for collisional ionization. The CLR is much smaller than the NLR (≈ 10", Fig. 4 and Marconi 1993) and the two regions must not necessarily be in pressure equilibrium. However, the difference in pressures found with a hot CLR is so large (a factor ≥ 40) as to require a confining medium for the CLR. In the case of photoionization the difference is modest and pressure equilibrium is roughly satisfied if the CLR has f close to unity. Therefore, a photoionized CLR with $f \simeq 1$ is the least demanding model from the dynamical point of view.

4.2. A photoionization model for the CLR

The temperature and ionization structure of the species of interest have been computed using CLOUDY (Ferland 1993). Line luminosities were then determined from the ionic distribution using the collision strengths of Blaha (1968), Mason (1975) and from the compilation of Kafatos & Lynch (1980). In all cases the models were spherically symmetric without any inner cut in radius and with constant density and filling factor. Element abundances were solar (He=10.99, Si=7.55, S=7.21, Ca=6.36, Fe=7.67 in the log(H)=12 scale) and without dust depletion (the results can be scaled to different metal abundances as Si, S, Ca and Fe are not dominant in the cooling). The number of Lyman continuum photons was varied within the range $Q(H) = 1 - 2 \cdot 10^{52}$ s^{-1} to be compatible with the luminosity distribution of Brγ derived from an IRSPEC map (Moorwood

& Oliva 1993b and work in preparation). For a given filling factor the density N_H was adjusted to match the observed flux and surface brightness of [Fe XI].

Having several pairs of lines from different ionization stages of the same element it is possible to constrain the absolute strength and shape of the ionizing field between the threshold energies, i.e. from 100 eV (Fe VII) to 329 eV (S IX). The ionization structure of the higher ionization species (Si IX, S VIII, S IX, Fe X, Fe XI) is governed by geometric dilution and their abundance ratios depend primarily on the shape of the input spectrum. Among the various combinations of line ratios we found that the least sensitive to other parameters is

$$\mathscr{R}(\mathrm{S,Fe}) = \frac{[\mathrm{S\ IX}]/[\mathrm{S\ VIII}]}{[\mathrm{Fe\ XI}]/[\mathrm{Fe\ X}]} \simeq 1.6 \cdot 1.25^{-\alpha(300)} \quad (3)$$

The simple formula on the right hand side works remarkably well* (within 10% over a broad range of conditions) although based on highly simplified considerations: 1.25 is the ratio between the ionization thresholds of S^{+7} and Fe^{+10}, and $\alpha(300)$ is the spectral slope between 262 and 328 eV ($L_\nu \propto \nu^{-\alpha(300)}$, $\alpha(300) \geq 0$). The observed value of $\mathscr{R}$(S,Fe) indicates $\alpha(300) \lesssim 1$, a surprisingly flat spectrum (see below).

The ionization structure of Fe VII (and to a lesser extent Si VI) is dominated by the continuum opacity of He^+ because R(He III), the radius of the He III Strömgren sphere, is smaller than the radius at which the relative abundance of Fe VII would peak for geometric dilution. In other words, the ionization parameter at R(He III) is still too large for Fe VII which however peaks there and does not extend beyond because $\tau(He^+)$ kills most of the photons which can photoionize Fe IV ($h\nu_{ion}$ = 57 eV). Therefore, R(He III) is effectively the size of the CLR and the lines of He II can be considered as 'coronal'. The intensity of [Fe VII] critically depends not only on the shape of the ionizing spectrum but also on all those parameters which determine the size of the He III sphere, i.e. $Q(He^+)$, N_H, A(He) and f. The contribution of [Ca V] λ6087 to [Fe VII] is negligible as the models predict [Ca V]/[Ca VIII]< 0.1 under any reasonable condition (see also Marconi et al. 1994).

By varying the parameters within reasonable limits we were able to obtain a good fit to the observed quantities. Table 2 lists the results of a toy model (PH1) with Q(H) = 10^{52} s^{-1}, N_H = 200 cm^{-3}, f = 1 and a double power-law spectrum with α_1=2 between 13.6 and 140 eV and α_2=0.5 beyond with a break at 700 eV to obtain a standard F_ν(1keV)/F_ν(10eV) ratio (e.g. Malkan & Sargent 1982). The small value of α_2 is necessary to match $\mathscr{R}$(S,Fe) (Eq. 3) and the intensities of the highest ionization lines; particularly critical is the ratio [Si IX]/[Si VII]. The steeper slope between 13.6 and 54.4 eV is required to obtain the correct size of the He III Strömgren sphere and models with much shallower α_1 predict too much [Fe VII] and He II. Models with smaller f require larger densities to conserve the flux and surface brightness of the lines ($N \propto f^{-1/2}$, Sect. 4.1). The increased density produces a lower ionization degree at a given distance from the nucleus which can only be compensated by a further hardening of the spectrum. In practice, we were unable to find any reasonable combination of parameters which could fit the observed line ratios with $f < 0.1$. This is another piece of evidence in favour of $f \simeq 1$ in the CLR.

The basic conclusion from the modeling is that the ionizing spectrum must be very flat between 150 and 350 eV. This indicates that the continuum at these energies is much harder than presently believed and excludes the warmer model of Terlevich & Melnick (1985) whose ionizing spectrum has a sharp cut-off at about 300 eV. To better evaluate this point we computed a model (PH2) using the 'standard AGN continuum' of CLOUDY and Q(H)=2 $\cdot$ 10^{52} s^{-1}. Compared to PH1 this has more Lyman continuum photons and is slightly flatter before the He^+ threshold but is far too steep between 55 and 350 eV and fails to reproduce the higher ionization lines; note in particular the large difference in [Si IX]/[Si VII]. The difficulty of making this ratio greater than unity in gas photoionized by hot stars is also evident from the spectra of the high excitation planetary nebula NGC6302, whose exciting star is hotter than 2 10^5 K and which emits strong [Si VII] but no detectable [Si IX] (cf. fig. 2 of RO93).

The XUV spectrum which we deduce for the Circinus galaxy doesn't seem to be typical. We find a rather steep decline just above 1 Rydberg, and this would exacerbate the "missing energy problem" pointed out by Netzer (1985); we also find a flat distribution around 0.2-0.4 keV, where instead many AGNs are observed to have extremely soft "excesses" (see, e.g., Elvis 1989). Many more nuclei must be studied in comparable detail before statistical conclusions can be drawn.

Concerning element abundances it appears that S, Si, Ca and Fe have abundances close to solar: [Fe VII]/He II is compatible with a normal Fe/He, Fe/S (from [Fe X]/[S VIII]) is low by a factor $\sim$ 1.5 while Si/S (from [Si VII]/[S VIII]) and Ca/Si (from [Ca VIII]/[Si VII]) are up by a similar factor. Apart from these details the crucial result is that refractory elements (Si, Ca, Fe) are not significantly depleted with respect to sulphur and helium and hence there is no evidence for the presence of refractory dust in the CLR. Considering that grains made of Si/Fe are much more difficult to destroy than other kinds of dust it appears likely that the CLR is essentially dust free.

4.3. A collisionally ionized model for the CLR

A coronal gas is, by definition, a hot plasma where the most important process for ionization is electron collisions while photoionization is negligible. Under these conditions the ionization state of the gas follows from the statistical equilibrium between collisional ionizations and radiative plus dielectronic recombinations, and is solely determined by the gas temperature T (e.g. Jordan 1969). Values of $x(X^{+i})$ (the ionization fraction of a given species X^{+i}) as a function of T have been computed and tabulated in the above reference and subsequently updated by various authors (e.g. Landini & Monsignori Fossi 1971; Shull

* Eq. 3 has general validity as long as the ionization structure is dominated by geometric dilution, i.e. up to values of the parameter $\Xi = Q(\mathrm{H})\, N\, f^2$ (Marconi et al. 1994) of a few $\times 10^{56}$

Table 2. Coronal lines: comparison between models and observations

Parameter	observed	PH1[a]	PH2[a]	COL[a]
F_{-15}[Fe XI]	110±25[b]	93[b]	80[b]	–
σ_{-13}[Fe XI]	3.1±1[c]	2.9[c]	3.1[c]	–
[Fe VII]/[Fe X]	.47±.08	0.44	2.45	–
[Fe XI]/[Fe X]	.65±.10	0.72	0.54	0.74
[Fe XIV]/[Fe X]	< 1	0.24	0.11	0.02
[Si VII]/[Si VI]	1.61±.24	1.38	0.72	1.77
[Si IX]/[Si VII]	1.32±.20	1.13	0.18	1.20
[S IX]/[S VIII]	0.96±.15	1.00	0.34	0.91
[Fe X]/[S VIII]	2.36±.33	3.19	2.90	10.2
[Ca VIII]/[Si VII]	0.46±.06	0.27	0.28	–
[Si VII]/[S VIII]	3.24±.50	2.24	4.13	1.57
He II/[Fe VII]	5.4±1.6	3.99	2.07	–

Notes to Table 2

[a] PH1: best photoionized, PH2: photoinized by standard AGN continuum, COL: best collisionally ionized. All models assume solar abundances, i.e. He=10.99, Si=7.55, S=7.21, Ca=6.36, Fe=7.67 in the log(H)=12 scale. See sect. 4.2, 4.3 for details.

[b] Line intensity in 10^{-15} erg cm^{-2} s^{-1}

[c] Surface brightness in 10^{-13} erg cm^{-2} s^{-1} arcsec^{-2}.

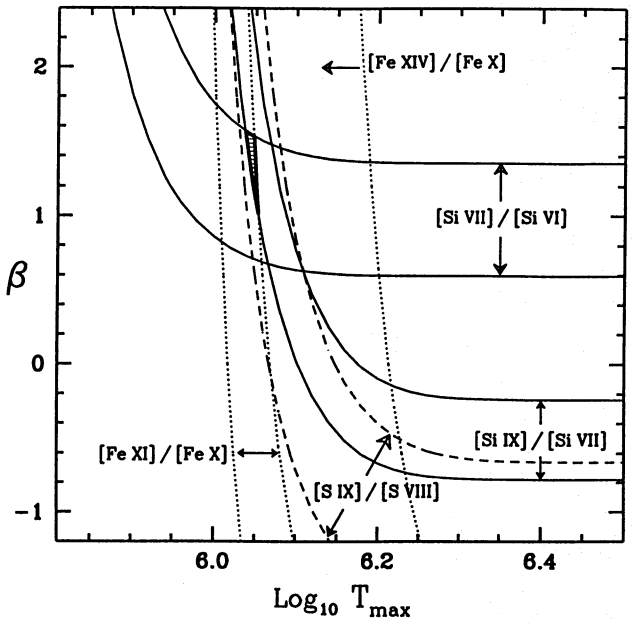

Fig. 5. Predicted line ratios from a a model of hot, collisionally ionized gas as a function of T_{max} (the upper cut in temperature for the gas distribution) and β (the slope of the temperature distribution). The curves show the loci compatible with the observed line ratios. The small, dashed area gives the range of parameters which can reproduce the observed values; see Sect. 4.3 for more details

& van Steenberg 1982), we adopted the most recent results of Monsignori Fossi & Landini (1993).

In a coronal gas the kinetic energy of electrons and protons is comparable to $h\nu_{ion}$, the ionization potential of a given ion. Consequently, the line formation is dominated by direct proton collisions to "u" (the upper level of the observed transition), and electron excitations of high lying states which cascade to "u", these are particularly important for Fe ions (e.g. Mason 1975). The rates for proton excitations were taken from Bely & Faucher (1970) and Landman (1980), while the atomic parameters for electron collisions to high levels were from Aggarwal & Kingston (1986), Bhatia et al. (1979), Mason (1975), Mason & Bhatia (1978), Mohan et al. (1987), Mohan & Le Dourneuf (1990). We could determine line emission coefficients for all the ions of interest except Ca VIII and Fe VII which were therefore excluded from the computation.

We adopted a multi–temperature model where the various regions have emission measures $EM = N^2 V$ distributed according to a power law, $EM(T) \propto T^{\beta}$, cut at T_{min} and T_{max}, an approach similar to that of NO70. We constructed a grid of models at different β, T_{min} and T_{max} with the following results.

– The choice of T_{min} has little influence on the lines under consideration, the only constraint on this parameter comes from [Si VII]/[Si VI] which requires $T_{min} \lesssim 4 \cdot 10^5$ K.

– The ratio [Si VII]/[Si VI] depends primarily on β, the observed value yields $0.5 < \beta < 1.5$.

– [S IX]/[S VIII], [Si IX]/[Si VII] and [Fe XI]/[Fe X] critically depend on the choice of T_{max}. The observed line ratios can be reproduced using $T_{max} \simeq 1.1 \cdot 10^6$ K but increase by more than a factor of 2 just going to $T_{max} = 1.6 \cdot 10^6$ K; above $T_{max} > 2 \cdot 10^6$ K one also predicts too much [Fe XIV], an effect already noticed by NO70.

These considerations are summarized in Fig. 5 which shows the loci of the T_{max}–β plane compatible with the observed line ratios. There is a small region ($1.09 \cdot 10^6 < T_{max} < 1.14 \cdot 10^6$ and $1 < \beta < 1.5$) where the model is able to reproduce the observations, the best–fit values are for $T_{max} = 1.115 \cdot 10^6$ K and $\beta = 1.35$ and are listed in Table 2, last column. The choice of T_{max} is arbitrary, however, and there is no obvious physical process which could produce a sharp cut in the gas distribution at such a finely tuned temperature.

Another characteristic of the model is to predict (regardless of the choice of T_{min}, T_{max} and β) too strong [Fe] lines with respect to [S] and [Si]. This is due to the fact that Fe ions have much more levels within $E/k \approx 10^6$ K from the ground state which can be excited by electron collisions at coronal temperatures and contribute to the emissivity of the observed lines; for example the ratio ϵ(Fe X)/ϵ(S VIII) increases by almost a factor of 3 going from $T = 3 \cdot 10^4$ K to $T = 8 \cdot 10^5$ K.

In conclusion one finds that a 'typical', collisionally ionized gas should be characterized by [Si IX]/[Si VII], [S IX]/[S VIII], [Fe XI]/[Fe X] and [Fe]/[S] ratios much larger than those observed. However, by decreasing the Fe/S relative abundance and cutting the gas temperature distribution at a carefully chosen, *ad hoc* value one can still fit the observations.

4.4. The possible contribution from a low density CLR

The above results add support to the proposal of KF89 that the CLR is 'normal' gas photoionized by an active nucleus except for the much higher density which we require. KF89 argued that the coronal lines may form in a typical, low density ($N_e \sim 1$) interstellar medium exposed to the hard nuclear continuum. The problem with such a model is that the line emission is very extended and its surface brightness is orders of magnitudes below that found in this and other galaxies where the CLR is spatially unresolved (Colina 1992). Specifically, the model of KF89 for NGC4151 with $N_e = 1$ predicts a diameter of the Fe VII region $\theta \simeq 34$", a line surface brightness of $3.5 \cdot 10^{-17}$ erg cm^{-2} s^{-1} arcsec^{-2} (close to the limit of the most sensitive spectrographs), and a [Fe VII] flux in the central 4"x4" a factor ~ 200 lower than that measured by Veilleux (1988) in a similar aperture. The situation rapidly improves in models with larger densities as the average ionization degree roughly increases as $N_e^{1/3}$ (Oliva & Panagia 1983) while $\theta \approx N_e^{-2/3}$. Still, the highest density ($N_e = 10$) model of KF89 has an easily resolvable CLR ($\theta \sim 8$") and densities of at least 100 cm^{-3} are required to push its size below 2".

The same arguments apply to a low density coronal gas at $T \sim 10^6$ K which may be the confining medium for the NLR clumps (Oke & Sargent 1969). In the Circinus galaxy the surface brightness of coronal lines from such a medium would be more than 3 orders of magnitude lower than observed. More generally one can easily verify that the intensities of [Fe XI] and other coronal lines from a diffuse and hot gas in pressure equilibrium with the NLR are at most a fraction $10^{-5}/f_{\rm NLR}$ of the Hα emitted by the NLR clumps, $f_{\rm NLR}$ being their filling factor. These very faint lines would be extremely difficult to detect over the strong galactic continuum.

5. Conclusions

Our study of visible ([Fe VII], [Fe X], [Fe XI], [S VIII]) and near infrared ([S IX], [Si VI], [Ca VIII], [Si VII], [Si IX]) coronal lines in the Circinus galaxy can be summarized as follows.

– The presence of these lines confirms that this galaxy hosts one of the nearest (D$\simeq$4 Mpc) Seyfert nuclei. [S IX]1.252μm ($h\nu_{ion}$=329eV) is a newly detected astronomical line and our measurement of [Si IX]3.935μm ($h\nu_{ion}$=303eV) is the first in an extragalactic object. This latter is both the brightest and longest wavelength of the detected lines and could hence offer a valuable diagnostic probe of Seyfert activity in visually obscured AGNs.

– The coronal line region (CLR) is very compact but spatially resolved; the diameter of the [Fe XI] emitting region is $\simeq$10 pc.

– The lines are narrow ($\leq$100 km/s) and hence exclude the possibility that the coronal gas is produced by fast ($v \geq 300$ km/s) shocks.

– The surface brightness of the lines implies that the CLR is quite dense: $N_e \simeq 250\, f^{-1/2}$ where f is the filling factor; several arguments indicate that $f \simeq 1$.

– The line ratios are consistent with photoionization by a double power law continuum whose slope around 300 eV can be analytically estimated from ([S IX]/[S VIII])/([Fe XI]/[Fe X]). This yields a flatter spectrum at these energies than currently believed and one that cannot e.g. be generated by hot stars alone (warmers).

– The relative abundances of He, Si, S, Ca and Fe are close to their solar values implying little or no depletion of refractory elements and hence no dust in the CLR.

– Models of collisionally ionized gas predict [S IX]/[S VIII], [Si IX]/[Si VII] and [Fe XI]/[Fe X] much larger than observed unless one introduces a sharp cut in the temperature distribution just above 10^6 K, and only with a careful tuning ($T_{max} = 1.115 \pm 0.025 \cdot 10^6$ K) can one reproduce the observed line ratios. This *ad hoc* choice has no physical ground and makes it unlikely that a hot, coronal, plasma is the source of these lines.

Acknowledgements. This work is based on a part of the thesis work by A. Marconi.
We are grateful to M. Landini and B. Monsignori Fossi for useful discussions and comments. We thank G. Ferland for making available his code to the community.

References

Aggarwal K.M., Kingston A.E., 1986, A&A 162, 333
Bhatia A.K., Feldman U., Doscheck G.A., 1979, A&A 80, 22
Bely O., Faucher P., 1970, A&A 6, 88
Blaha M., 1968, Ann. Astrophys. 31, 311
Colina L., 1992, ApJ 386, 59
Contini M., Viegas S.M., 1992, ApJ 401, 481
Davidson K., Netzer H., 1979, Rev. of Modern Phys. 51, 715
Elvis M., 1989, Comments on Astrophysics 14, 177
Ferland G.J., 1993, University of Kentucky Department of Physics and Astronomy Internal Report
Freeman C., Karlsson B., Lynga G., Burrel J.F., van Woerden H., Gross W.M., Mebold U., 1977, A&A 55, 445
Fuhr J.R., Martin G.A., Wiese W.L., 1988, J. Phys. Chem. Ref. Data 17, Suppl. 4
Gardner F.F., Witheoak J.B., 1982, MNRAS 201, 13p
Grandi S.A., 1978, ApJ 221, 501
Jordan C., 1969, MNRAS 142, 501
Kafatos M., Lynch J.P., 1980, ApJS 42, 611
Korista K.T., Ferland, G.J., 1989, ApJ 343, 678 (KF89)
Landman D.A., 1980, ApJ 240, 709
Landini M., Monsignori Fossi B.C., 1971, A&AS 7, 291
Malkan M.A., Sargent W.L.W, 1982, ApJ 254, 22
Marconi A., 1993, Thesis, University of Florence
Marconi A., Moorwood A.F.M., Salvati M., Oliva E., 1994, submitted to A&A
Mason H.E., 1975, MNRAS 170, 651
Mason H.E., Bhatia A.K., 1978, MNRAS 184, 423
Mohan M., Baluja K.L., Hibbert A., 1987, J. Phys. B 20, 2565
Mohan M., Le Dourneuf M., 1990, A&A 227, 285
Monsignori Fossi B.C., Landini M., 1993, private communication
Moorwood A.F.M., Glass I.S., 1984, A&A 135,281
Moorwood A.F.M., Moneti A., Gredel R., 1991, The Messenger 63, 77
Moorwood A.F.M., Oliva E., 1988, A&A 203, 278
Moorwood A.F.M., Oliva, E., 1990, A&A 239, 78

Moorwood A.F.M., Oliva, E., 1991, The Messenger 63, 57
Moorwood A.F.M., Oliva, E., 1993a, In 'Astronomical Infrared Spectroscopy', (ed. S. Kwok), PASP Conference Series 41, 305
Moorwood, A.F.M., Oliva E., 1993b, In CIRP5: Topical Conference on Infrared Astrophysics (ed. F.K. Kneubühl), Infrared Physics (in press).
Moorwood A.F.M., Origlia L., 1990, In Astrophysics with Infrared Arrays (ed. R. Elston), Astronomical Society of the Pacific Conference Series 14, 85
Netzer H., 1985, ApJ 289, 451
Nussbaumer H., Osterbrock D.E., 1970, ApJ 161, 811 (NO70)
Oliva E., Panagia N., 1983, Astrophys. and Space Science 94, 437
Oliva E., Moorwood A.F.M., Danziger I.J., 1989, A&A 214, 307
Oliva E., Moorwood A.F.M., 1990, ApJL 348, L5
Oliva E., Origlia L., 1992, A&A 254, 466
Oke J.B., Sargent W.L.W., 1969, ApJ 151, 807
Osterbrock D.E., Shaw R.A., Veilleux S., 1990, ApJ 352, 561
Osterbrock D.E., Martel A., 1992, P.A.S.P. 104, 76
Penston M.V., Fosbury R.A.E., Boksenberg A., Ward M.J., Wilson A.S., 1984, MNRAS 208, 347
Reconditi M., Oliva, E., 1993, A&A 274, 662 (RO93)
Shull M., van Steenberg, 1982, ApJS 48, 95
Smits D.P., 1991, MNRAS 248, 193
Terlevich R., Melnick, J., 1985, MNRAS 213, 841
Viegas-Aldrovandi S.M., Contini, M., 1989, A&A 215, 253
Veilleux S., 1988, AJ 95, 1695

This article was processed by the author using Springer-Verlag TEX A&A macro package 1992.